High-Order Large Eddy Simulation of Premixed Turbulent Flames

Luiz Tobaldini Neto

University of Toronto
Institute for Aerospace Studies

Doctoral Examination Committee
Meeting 4
November 10, 2014

Motivation

- Fossil fuels remain the principal sources of energy worldwide until 2035 and renewables grow rapidly [IEA, 2012];
- Combustion: very high energy density, fast transformation
- Aeronautics, Energy Generation, Automotive Engines...;
- Many efforts in green energy include/count on combustion systems (biofuels);
- Efficient combustion simulation: important role in systems design and emissions controls;
- Practical combustion devices are all turbulent;
- Complex features: (**chemistry + turbulence + geometry**);
- **High-order schemes** can bring **cost reduction**, **higher fidelity** to combustion simulations;

Literature Review

- High-Order(HO): typically for Direct Numerical Simulation (DNS), structured grids. Practical Large Eddy Simulation (LES): 2^{nd} or 3^{rd} accurate [van der Hoeven *et al*, 2007, Albouze *et al*, 2009, Poinsot, 2010];
- Franzelli *et al*[2012] use 3^{rd}-order Finite Elements(FE) for combustion instabilities on a swirled combustor;
- High Order-LES, Finite Differences (FD) for CH_4 combustion [Yaldizli *et al*, 2010]
- 5^{th}-order FD: gaseous detonations [Wang *et al*, 2012];
- 2^{nd}-order, LES Finite Volumes: combustion in gas turbines [Fureby, 2009];
- High-Order Discontinuous Galerkin for combustion [Lv and Ihme, 2013];

To our knowledge not much has been done in high order finite volume LES for combustion.

Proposal

Existing Framework

- Parallelization and AMR for RANS by Gao [2008];
- 2D High-Order (4th) by Ivan and Groth [2011];
- 3D High-Order (4th) structured [Ivan *et al*, 2012] and unstructured [Charest *et al*, 2012]
- PCM-FPI: LES by Hernàndez-Pérez *et al*[2010], RANS by Jha and Groth [2011];

This Research

3D finite volume scheme using high-order LES turbulence model and tabulated chemistry to simulate turbulent premixed flames.

Filtered Governing Equations

$$\frac{\partial \bar{\rho}}{\partial t} + \frac{\partial(\bar{\rho}\tilde{u}_j)}{\partial x_j} = 0\,, \tag{1}$$

$$\frac{\partial(\bar{\rho}\tilde{u}_i)}{\partial t} + \frac{\partial(\bar{\rho}\tilde{u}_i\tilde{u}_j + \delta_{ij}\bar{p})}{\partial x_j} - \frac{\partial \check{\tau}_{ij}}{\partial x_j} = \bar{\rho}g_i + \underbrace{\frac{\partial \sigma_{ij}}{\partial x_j}}_{\mathrm{I}} + \underbrace{\frac{\partial(\bar{\tau}_{ij} - \check{\tau}_{ij})}{\partial x_j}}_{\mathrm{II}}\,, \tag{2}$$

$$\begin{aligned}
\frac{\partial(\bar{\rho}\tilde{E})}{\partial t} + \frac{\partial[(\bar{\rho}\tilde{E} + \bar{p})\tilde{u}_j]}{\partial x_j} - \frac{\partial(\check{\tau}_{ij}\tilde{u}_i)}{\partial x_j} + \frac{\partial \check{q}_j}{\partial x_j} \quad = \quad & \bar{\rho}\tilde{u}_i g_i - \underbrace{\frac{\partial[\bar{\rho}(\widetilde{h_{\mathrm{s}} u_j} - \check{h}_{\mathrm{s}}\tilde{u}_j)]}{\partial x_j}}_{\mathrm{III}} \\
& + \underbrace{\frac{\partial(\overline{\tau_{ij} u_i} - \check{\tau}_{ij}\tilde{u}_i)}{\partial x_j}}_{\mathrm{IV}} - \underbrace{\frac{\partial(\bar{q}_j - \check{q}_j)}{\partial x_j}}_{\mathrm{V}} - \underbrace{\frac{1}{2}\,\frac{\partial[\bar{\rho}(\widetilde{u_j u_i u_i} - \tilde{u}_j\widetilde{u_i u_i})]}{\partial x_j}}_{\mathrm{VI}} \\
& - \underbrace{\frac{\partial[\sum_{\alpha=1}^{N} \Delta h^0_{\mathrm{f}_\alpha}\,\bar{\rho}(\widetilde{Y_\alpha u_j} - \tilde{Y}_\alpha\tilde{u}_j)]}{\partial x_j}}_{\mathrm{VII}}\,,
\end{aligned} \tag{3}$$

$$\frac{\partial(\bar{\rho}\tilde{Y}_\alpha)}{\partial t} + \frac{\partial(\bar{\rho}\tilde{Y}_\alpha\tilde{u}_j)}{\partial x_j} + \frac{\partial \check{\mathcal{J}}_{j,\alpha}}{\partial x_j} = -\underbrace{\frac{\partial[\bar{\rho}(\widetilde{Y_\alpha u_j} - \tilde{Y}_\alpha\tilde{u}_j)]}{\partial x_j}}_{\mathrm{VIII}} - \underbrace{\frac{\partial(\bar{\mathcal{J}}_{j,\alpha} - \check{\mathcal{J}}_{j,\alpha})}{\partial x_j}}_{\mathrm{IX}} + \underbrace{\bar{\dot{\omega}}_\alpha}_{\mathrm{X}}\,, \tag{4}$$

PCM-FPI - Chemistry Model

Flame Prolongation of Intrinsic Low-Dimensional Manifold (FPI) [Gicquel *et al*, 2000] combined with PCM - Presumed Conditional Moments [Vervisch *et al*, 2004]

- Create tables of φ_j^{FPI}=(Y_j or $\dot{\omega}_j$) from detailed simulations of simple flames (premixed, steady-state, 1D, laminar);
- Selected species (10): 99% of mass, energy and heat release;
- Map φ_j^{FPI} to Y_{c}-space.
- $\tilde{\dot{\omega}}_\alpha = f(\dot{\omega}_\alpha$,**presumed PDF for the scalar fluctuations**);
- Different PDFs possible, in this work: β-PDF, modified laminar flamelet based (MLPDF) [Jin *et al*, 2008];
- Solve transport equations for the progress of reaction variable and its variance;

High-Order Finite-Volume Formulation

Integral Form of the Governing Equations

$$\frac{\mathrm{d}\overline{\mathbf{U}}}{\mathrm{d}t} = -\frac{1}{V}\oiint_{A} \left(\vec{\mathcal{F}}^{\mathrm{I}} - \vec{\mathcal{F}}^{\mathrm{V}}\right) \cdot \hat{n}\mathrm{d}\mathcal{A} + \overline{\mathbf{S}}.$$

Using a two-dimensional Gauss quadrature integration rule:

$$\frac{\mathrm{d}\overline{\mathbf{U}}_{ijk}}{\mathrm{d}t} = -\frac{1}{V_{ijk}}\sum_{l=1}^{N_f}\sum_{m=1}^{N_G}\left(\omega\left(\vec{\mathcal{F}}^{\mathrm{I}} - \vec{\mathcal{F}}^{\mathrm{V}}\right) \cdot \hat{n}A\right)_{ijk,l,m} + \overline{\mathbf{S}}_{ijk} = \overline{\mathbf{R}}_{ijk}\left(\overline{\mathbf{U}}\right)$$

- Solution reconstruction
- Interface flux evaluation
- Source vector evaluation
- Time marching

Solution Reconstruction

- Reconstruction: *to assume some form of spatial distribution* of solution quantities in each cell, $\mathbf{U}_{ijk}(\vec{x})$,

$$\mathbf{U}_{ijk}^{k}(\vec{x}) = \sum_{\substack{p_1=0 \\ (p_1+p_2+p_3\leq k)}}^{k} \sum_{p_2=0}^{k} \sum_{p_3=0}^{k} (x - x_{ijk})^{p_1} (y - y_{ijk})^{p_2} (z - z_{ijk})^{p_3} D_{p_1 p_2 p_3} + \mathcal{O}\left(\Delta^{k+1}\right)$$

where

$$D_{p_1 p_2 p_3} = \frac{1}{p_1! p_2! p_3!} \frac{\partial^{p_1} U}{\partial x^{p_1}} \frac{\partial^{p_2} U}{\partial y^{p_2}} \frac{\partial^{p_3} U}{\partial z^{p_3}}$$

- Piecewise-constant reconstruction: $k = 0$;
- Piecewise-linear reconstruction: $k = 1$;
- Higher-order k-exact reconstructions: $k \geq 2$;
- For $k \geq 1$, solution monotonicity needs to be enforced.

- CENO uses fixed central stencil for reconstruction;
- Near discontinuities, under-resolved regions high-order k-exact reconstruction produces oscillatory behaviour;
- Smoothness indicators decide whether high-order k-exact reconstruction is used in a cell;
- Near discontinuities, CENO scheme is reverted to limited piecewise-linear reconstruction

$$\mathcal{S} = \frac{\gamma}{\max\left((1-\gamma), \epsilon\right)} \frac{(M-N)}{(N-1)},$$

$$\gamma = 1 - \frac{\sum_\beta \left(U_\beta^k(x_\beta, y_\beta, z_\beta) - U_\alpha^k(x_\beta, y_\beta, z_\beta) \right)^2}{\sum_\beta \left(U_\beta^k(x_\beta, y_\beta, z_\beta) - \overline{U}_\alpha \right)^2}.$$

Generic Hexahedral - Trilinear Transformation

- Use Gauss-Legendre quadrature rules, as defined on a Cartesian reference domain (cube);
- Transform points and weights from reference space (Cartesian) into physical space (hexahedral) using a trilinear description;

$$\vec{r}(p,q,r) = \vec{A} + \vec{B}p + \vec{C}q + \vec{D}r + \vec{E}pq + \vec{F}pr + \vec{G}qr + \vec{H}pqr \quad (5)$$

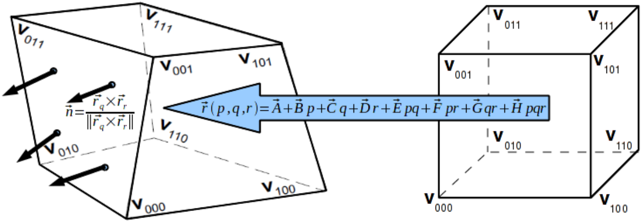

Figure: from Ivan et al. [2012]

Trilinear Transformation - Volumetric Integral

$$\mathcal{I} = \int_0^1 \int_0^1 \int_0^1 g(\vec{r}(p, q, r)) \det \mathbf{J} \, \mathrm{d}p \, \mathrm{d}q \, \mathrm{d}r \tag{6}$$

$$\mathcal{I} \simeq \sum_{m=1}^{N_{GV}} g\left(\vec{r}(p_m, q_m, r_m)\right) \left(\det \mathbf{J}\right)_m \omega_m = \sum_{m=1}^{N_{GV}} g(\vec{X}_m) \, \tilde{\omega}_m \tag{7}$$

- $\vec{X}_m = \vec{r}(p_m, q_m, r_m)$ - GL abscissa in physical space;
- $\tilde{\omega}_m = (\det \mathbf{J})_m \, \omega_m$ - weight in physical space.

Trilinear Transformation - Surface Integral

Example for constant $r=1$;

$$\mathcal{I}_{\text{face}} = \int_0^1 \int_0^1 g(\vec{r}(p,q,1)) \left| \frac{\partial \vec{r}}{\partial p} \times \frac{\partial \vec{r}}{\partial q} \right| \mathrm{d}p \, \mathrm{d}q \tag{8}$$

$$\mathcal{I}_{\text{face}} \simeq \sum_{m=1}^{N_{GF}} g\left(\vec{r}(p_m, q_m, 1)\right) \left(\mathbf{J}_{\text{face},m}\right) \omega_f = \sum_{m=1}^{N_{GF}} g(\vec{X}_m)\, \tilde{\omega}_m \tag{9}$$

- $\mathbf{J}_{\text{face},m} = \left(\left| \frac{\partial \vec{r}}{\partial p} \times \frac{\partial \vec{r}}{\partial q} \right| \right)_m$
- $\vec{X}_m = \vec{r}(p_m, q_m, 1)$ - GL abscissa in physical space;
- $\tilde{\omega}_m = (\det \mathbf{J})_m \, \omega_m$ - weight in physical space.

Inviscid Flux Evaluation

$$\frac{\mathrm{d}\overline{\mathbf{U}}_{ijk}}{\mathrm{d}t} = -\frac{1}{V_{ijk}} \sum_{l=1}^{N_f} \sum_{m=1}^{N_{GF}} \left(\tilde{\omega}_m \left(\vec{\mathcal{F}}^{\mathrm{I}} - \vec{\mathcal{F}}^{\mathrm{V}} \right) \cdot \hat{n} \right)_{ijk,l,m} + \overline{\mathbf{S}}_{ijk} = \overline{\mathbf{R}}_{ijk} \left(\overline{\mathbf{U}} \right)$$

- At a quadrature point in each cell interface, a Riemann problem must be solved
- $\vec{\mathcal{F}}^{\mathrm{I}} \cdot \hat{n} = \vec{\mathcal{F}}^{\mathrm{I}} \left(\mathbf{U}_{\mathrm{left}}, \mathbf{U}_{\mathrm{right}}, \hat{n} \right)$
- AUSM$^+$-up [Liou (2006)]

Viscous Flux Evaluation

$$\frac{\mathrm{d}\overline{\mathbf{U}}_{ijk}}{\mathrm{d}t} = -\frac{1}{V_{ijk}} \sum_{l=1}^{N_f} \sum_{m=1}^{N_{GF}} \left(\tilde{\omega}_m \left(\vec{\mathcal{F}}^{\mathrm{I}} - \vec{\mathcal{F}}^{\mathrm{V}} \right) \cdot \hat{n} \right)_{ijk,l,m} + \overline{\mathbf{S}}_{ijk} = \overline{\mathbf{R}}_{ijk} \left(\overline{\mathbf{U}} \right)$$

- At each quadrature point in a cell interface $(i + \frac{1}{2}, j, k)$:

$$\vec{\mathcal{F}}^{\mathrm{V}}_{i+\frac{1}{2},j,k} \cdot \hat{n} = \vec{\mathcal{F}}^{\mathrm{V}} \left(\mathbf{U}_{i+\frac{1}{2},j,k}, \vec{\nabla} \mathbf{U}_{i+\frac{1}{2},j,k} \right).$$

- Interface states and gradients are arithmetic mean of left and right states and gradients, respectively
- These states and gradients are reconstructed without limiting

$$U^k_{ijk}(x,y,z) = \sum_{\substack{p_1=0 \\ (p_1+p_2+p_3 \le k)}}^{k} \sum_{p_2=0}^{k} \sum_{p_3=0}^{k} (x - x_{ijk})^{p_1} (y - y_{ijk})^{p_2} (z - z_{ijk})^{p_3} D_{p_1 p_2 p_3} + \mathcal{O}\left(\Delta^{k+1}\right)$$

$$\frac{\partial U^k_{ijk}(x,y,z)}{\partial x} = \sum_{\substack{p_1=1 \\ (p_1+p_2+p_3 \le k)}}^{k} \sum_{p_2=0}^{k} \sum_{p_3=0}^{k} p_1 (x - x_{ijk})^{p_1-1} (y - y_{ijk})^{p_2} (z - z_{ijk})^{p_3} D_{p_1 p_2 p_3} + \mathcal{O}\left(\Delta^{k}\right)$$

Research Progress

DEC I

- Preliminary works with Trilinear Transformation and Gauss Quadrature

DEC II

- Function Reconstructions/Euler in non-Cartesian meshes
- Extension of CENO High-Order to non-reactive LES solver
- Application to Isotropic Turbulence Decay

DEC III

- Extension CENO High-Order to reactive LES solver (PCM-FPI)
- Application to Freely Propagating Flame in a 3D Cartesian Box

Planned Work for DEC IV

- High Order PCM-FPI Code Optimization (evolution of preliminary implementation used last year to avoid unnecessary Reconstructions)
- Application of the method to laboratory premixed Bunsen-type flame
- Cost Assesment: fourth-order compared to second-order;

Code Optimization

- Initial version of the PCM-FPI implementation relied on the reconstruction machinery for all variables (8 transported + 10 species);
- Idea of limiting the use of reconstruction machinery only to transported variables (8);
  - Read species mass fractions from tables instead of reconstructing;
  - Requires updating species from tables after block communications;
  - Use of chain rule for species spatial derivatives;
  - Measured gains on the order of 30%-40%;
  - Similar modifications extended to second-order code;

Laboratory Scale Turbulent Premixed Burner

- Axisymmetric Bunsen-type burner of Yuen & Gülder (2009)
- 11.2 mm diameter burner nozzle, annular pilot flame
- Premixed methane/air & propane/air flames, range of fuel mixtures & turbulence intensities, atmospheric pressures
- Rayleigh scattering and PIV measurements

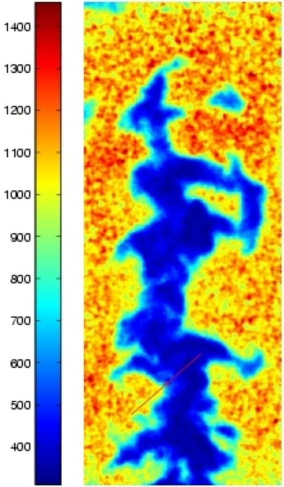

Computational Studies for Case N - Methane - ϕ =0.7

Λ	λ	η	u'	s_L	δ_L	u'/s_L	Λ/δ_L
mm	mm	mm	m/s	m/s	mm		
1.790	0.460	0.02935	2.92	0.201	0.11	14.38	16.64

Mesh Size	Spatial Order
200,000	2^{nd}, 4^{th}
690,000	2^{nd}, 4^{th}
1,600,000	2^{nd}, 4^{th}
6,400,000	2^{nd}

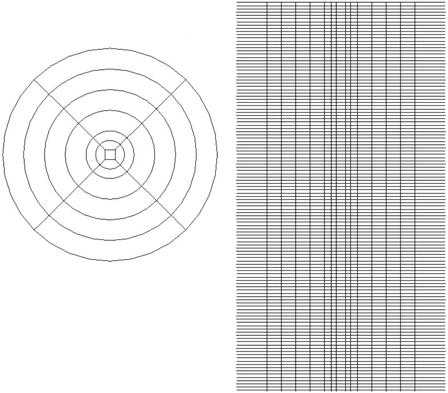

(a) XY (b) YZ

Flame Height vs. Mesh Size

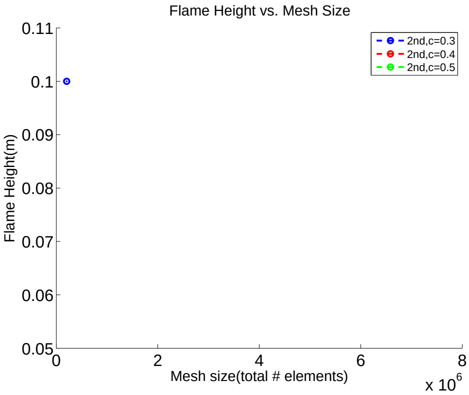

(c) Flame Height vs Mesh Size

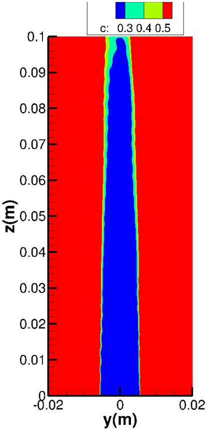

(d) 2^{nd} order, N=200,000 elements

Flame Height vs. Mesh Size

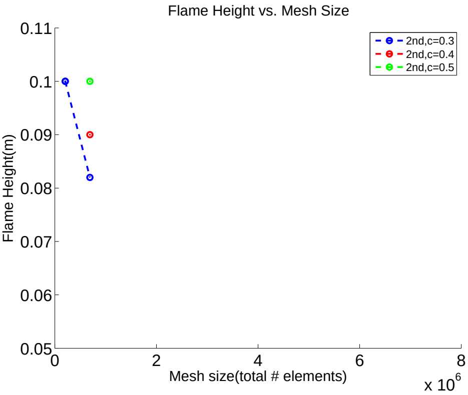

(e) Flame Height vs Mesh Size

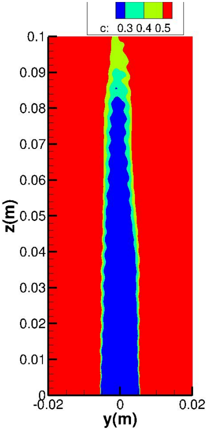

(f) 2^{nd} order, N=690,000 elements

Flame Height vs. Mesh Size

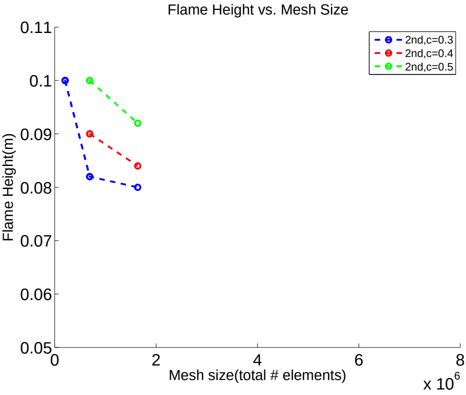

(g) Flame Height vs Mesh Size

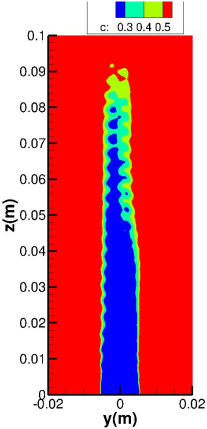

(h) 2^{nd} order, N=1,600,000 elements

Flame Height vs. Mesh Size

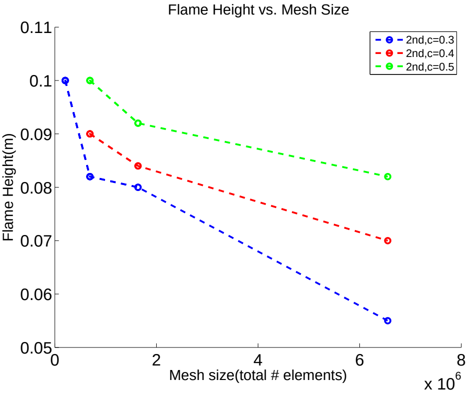

(i) Flame Height vs Mesh Size

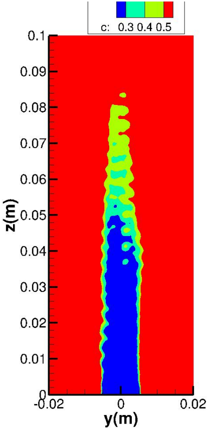

(j) 2^{nd} order, N=6,400,000 elements

Flame Height vs. Mesh Size

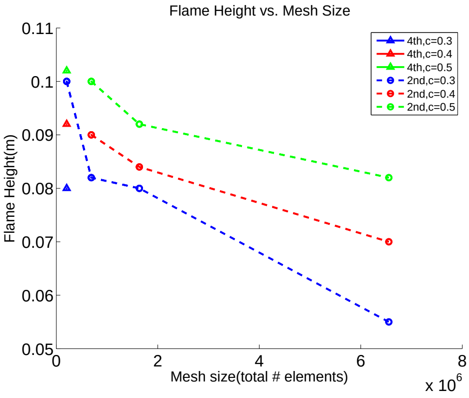

(k) Flame Height vs Mesh Size

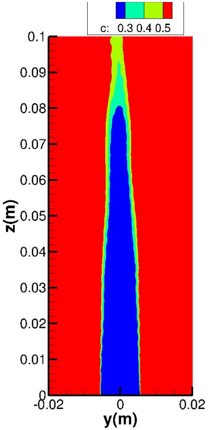

(l) 4^{th} order, N=200,000 elements

Flame Height vs. Mesh Size

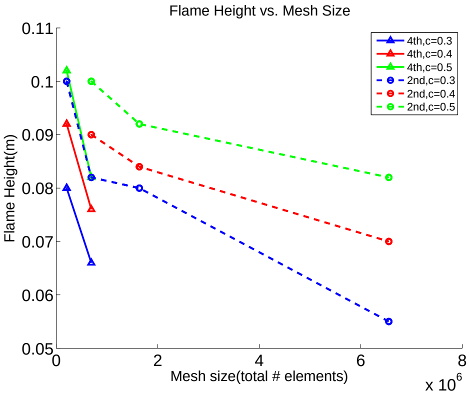

(m) Flame Height vs Mesh Size

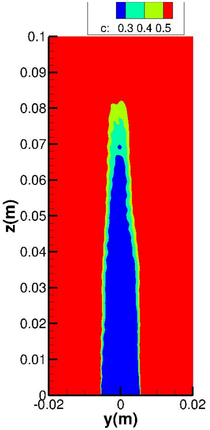

(n) 4^{th} order, N=690,000 elements

Flame Height vs. Mesh Size

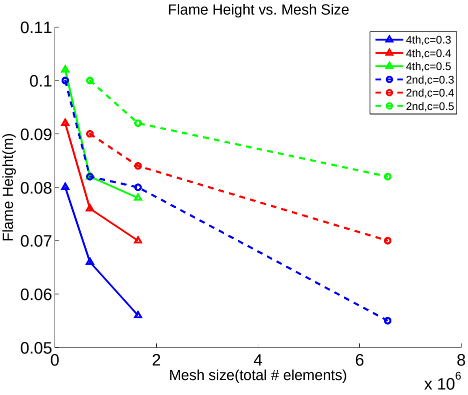

(o) Flame Height vs. Mesh Size

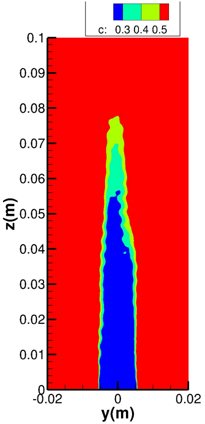

(p) 4^{th} order, N=1,600,000 elements

Error Relative to Experiment - $N^{1/3}$

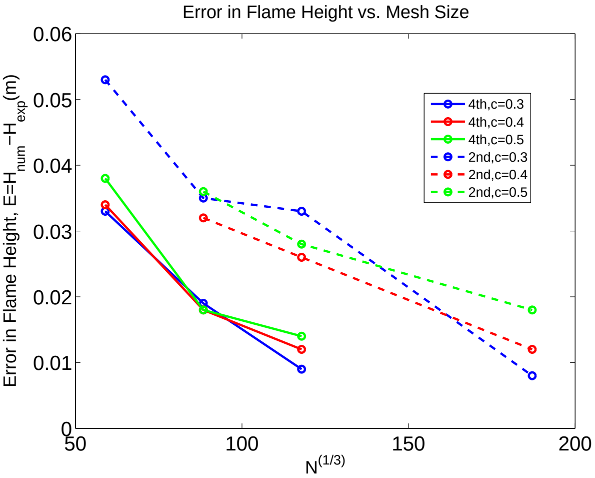

Avg. Error Relative to Experiment - $N^{1/3}$

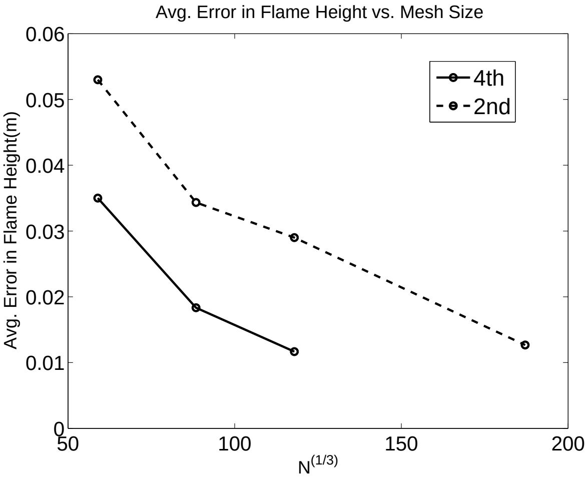

Avg. Error Relative to Experiment vs Cost RK4

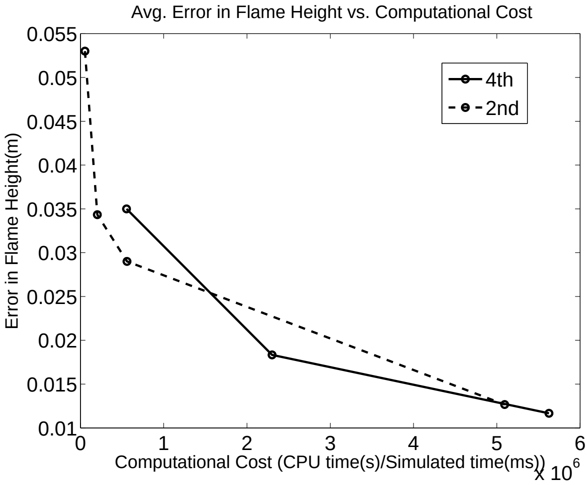

Avg. Error Relative to Experiment vs Cost RK2

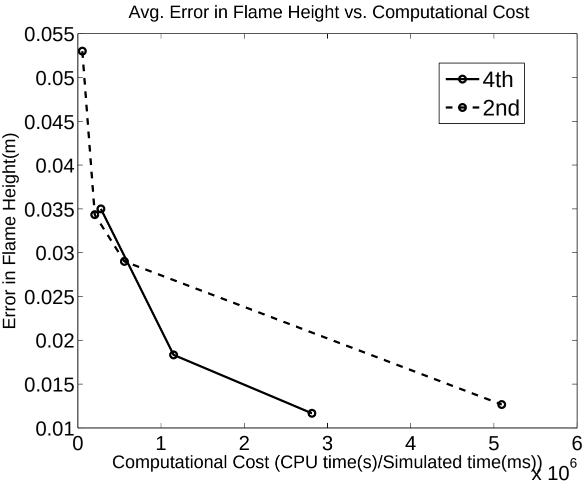

Conclusion

- Similar levels of representation of experimental results were obtained with second-order and fourth-order scheme. For this problem the effect of order of time-marching scheme was negligible in the results but substantial in cost;
- Substantial **gains in computational cost** can be realized **with the use of a high-order spatial discretization** to achieve the same level of representation of experimental results when compared to a second-order scheme;
- Same level of representation of experiments with coarser mesh $\rightarrow$ easier data management/post processing (more relevant for large number of cases);

Progress Since Previous Meeting

- Code optimization achieving 30-40% reduction in computational cost for the high-order framework;
- Extension to the second-order scheme of the applicable modifications made to the high-order framework;
- Application of the high-order framework to the simulation of a laboratory scale Bunsen burner.
- Mesh refinement study for the high-order and second-order schemes;
- Cost analysis of CENO high-order vs. second-order method showing substantial gains (**2-4 times less expensive**) in computational cost for same level of representation of experimental results;

1. AIAA - Scitech (January/2014 - National Harbour, MD, USA);
2. CI/CS Spring Meeting (May/2014 - Windsor, ON);
3. 22^{nd} Annual Conference CFDSC (June/2014 - Toronto, ON);

Summary of the contributions of the present work

- Collaboration in the implementation and testing of the trilinear transformation within the high-order framework, extending the ability of the code to handle non-orthogonal hexahedral elements;
- Extension of the high-order framework to handle reactive flows by implementing a high-order for the LES of turbulent premixed flames using the PCM-FPI model (tabulated chemistry coupled with a presumed PDF);
- First application of the compressible CENO high-order scheme to the LES of laboratory scale premixed flames (Bunser burner). To our knowledge this is one of the first applications of a high-order, classic (conservative, Godunov-type) compressible, finite-volume scheme to combustion problems;
- Performed a systematic cost assessment comparing the high-order scheme and second-order scheme using different mesh refinements for a premixed Bunsen burner laboratory flame, demonstrating the benefits of the high-order scheme in reducing the computational cost of these simulations and encouraging further research in this area;

Final Steps

- Run the mesh convergence study for the second-order scheme varying the filter width, having the filter/grid ratio constant;
- Spot checks for sensitivity analysis (cost vs. accuracy): *e.g.* vary number of volumetric quadrature points or FPI table size, test intermediate third-order spatial scheme;
- Organization of final thesis document (has been continuously conducted).

Acknowledgements

- Embraer S.A - Brazil;
- CNPq- Science Without Borders - Brazil;
- MITACS - Canada;
- Scinet (Computational Resources) - Canada;

Thank You!

Questions?

Turbulent Premixed Combustion

- Reactants perfectly mixed at the molecular level before entering reactor;
- Practical combustion devices are all turbulent;
- Turbulent flows $\rightarrow$ wide range of length and time scales

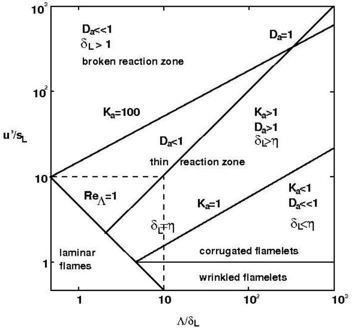

Λ = integral length scale

δ_{L} = laminar flame thickness

u' = RMS velocity fluctuation

s_{L} = laminar flame speed

$$Da = \frac{\Lambda / u'}{\delta_{\mathrm{L}} / s_{\mathrm{L}}}$$

$$Ka = \frac{\delta_{\mathrm{L}} / s_{\mathrm{L}}}{\eta / u'_{\mathrm{K}}}$$

η = Kolmogorov length scale

Regime diagram for premixed turbulent combustion

IEA. World Energy Outlook 2012. Technical report, International Energy Agency, 2012.

C. Fureby. Large eddy simulation modelling of combustion for propulsion applications. *Philosophical Transactions of the Royal Society of London A*, 367:2957–2969, 2009.

Y. Lv and M. Ihme. Higher-order discontinuous galerkin method for application to realistic combustion problems. In *14th International Conference on Numerical Combustion*, volume 32, San Antonio, USA, 2013.

X. Gao. *A Parallel Solution-Adaptive Method for Turbulent Non-Premixed Combusting Flows*. PhD thesis, University of Toronto, August 2008.

L. Ivan and C. P. T. Groth. High-order solution-adaptive central essentially non-oscillatory (CENO) method for viscous flows. Paper 2011-0367, AIAA, January 2011.

Pradeep Kumar Jha and Clinton P. T. Groth. Parallel adaptive mesh refinment scheme with presumed conditional moment and fpi tabulated chemistry for turbulent non-premixed combustion. Paper, AIAA, January 2011.

L. Ivan, A. Susanto, H. De Sterck, and C.P.T. Groth. High-order Central ENO finite-volume scheme for MHD on three-dimensional cubed-sphere grids. In *Seventh International Conference on Computational Fluid Dynamics (ICCFD7)*, page 1, July 2012.